Spectral Broadening and Pulse Compression in Molecular Gas-Filled Hollow-Core Fibers

Tran-Chau Truong, Christopher Lantigua, Yuxuan Zhang, Jack W. Agnes, Ruaridh Forbes, Bonggu Shim, and Michael Chini, *Member, IEEE*

(Invited Paper)

***Abstract*—Gas-filled hollow-core fibers have over the last three decades emerged as a key technology for ultrafast nonlinear optics and strong-field physics. Today, noble gas-filled capillary and microstructured fibers are used to generate broadband, coherent supercontinuum spectra through self-phase modulation, which can then be compressed to yield few-cycle driving pulses spanning the ultraviolet to mid-infrared. More recently, the use of molecular gases for spectral broadening has attracted significant interest, due to the interplay of the rotational and vibrational degrees of freedom with the electronic nonlinearity. Depending on the pulse duration of the driving laser, the complex interplay between instantaneous Kerr effect and the "delayed" rotational and vibrational Raman nonlinearities can induce novel behavior, such as four-wave mixing, stimulated Raman scattering, and soliton self-frequency shifting, which can combine with self-phase modulation to realize unique few-cycle sources in spectral regions inaccessible the laser gain medium. In this Invited Paper, we discuss new routes to spectral broadening in molecular gas-filled hollow-core capillary fibers, with a particular focus on the generation of few-cycle pulses from ytterbium-doped laser amplifiers. We review the physics underlying the rotational enhancement of optical nonlinearity in linear molecules and explore nonlinear propagation in molecular gas-filled fibers through both simulations and experiments. We demonstrate pulse compression, using dispersive mirrors and bulk media to produce few-cycle output pulses in different spectral regions, and discuss the challenges and opportunities for average power scaling. Finally, we describe the prospects for generating few-cycle sources in the mid-infrared through red-shifted broadening initiated by long-wavelength driving lasers.**

***Index Terms*—Attosecond, few-cycle, hollow-core fiber, laser, nonlinear optics, self-phase modulation, spectral broadening, ultrashort pulse.**

I. Introduction

THE generation and control of broadband coherent light across the electromagnetic spectrum has been an important enabling technology for the study of light-induced phenomena in matter. In recent decades significant effort has been spent on trying to understand light-matter interactions at increasing shorter timescales as well as higher intensities. Titanium-Sapphire laser systems, based on chirped pulses amplification [1], have represented the workhorse tool for the majority of these studies. Despite their prevalence, the utility of these lasers for studying ultrafast dynamics down to the few-femtosecond time scale is limited due to the typical pulse durations (∼30 fs) routinely available, which represent many optical cycles in the near infrared. For many light-driven processes the dynamics at the level of a single optical cycle play an important role; hence generating octave-spanning spectra is important for entering this regime [2]. A commonly used method for increasing the bandwidth of multicycle laser pulses is the propagation through a medium where the nonlinear process of self-phase modulation (SPM) is exploited to generate a supercontinuum [3].

One of the cornerstone techniques for generating single- or few-cycle laser pulses is to increase the bandwidth, via SPM, in a noble gas-filled hollow core fiber (HCF) and to compensate for the resulting dispersion via chirp mirrors [4]. This method, first introduced by Nisoli and coworkers [5], is now routinely used to generate the few-cycle laser pulses needed to produce attosecond pulses in the extreme ultraviolet (XUV) and X-ray through high-harmonic generation (HHG) [2]. Compared to other approaches, such as SPM induced via filamentation [6], [7] or bulk material [8], [9] the HCF method offers excellent beam quality, due to propagation of the light in a specific mode of the fiber, as well as a high degree of spectral uniformity across the beam profile [10]. The method is also scalable to relatively high pulse energies [11], [12] and, through the important development of stretched HCF to reduced transmission losses [13], scalable to longer wavelengths in the infrared (IR) [14], [15]. This desire to achieve few-cycle pulses in the IR is partially driven by the inherent scaling rule of the maximum photon energy generated in HHG, the so-called "cut-off" energy. The straightforward

Manuscript received 7 March 2024; revised 1 May 2024; accepted 2 May 2024. Date of publication 16 May 2024; date of current version 30 May 2024. This work was supported in part by the U.S. Department of Energy, Office of Science, Basic Energy Sciences under Grant DE-SC0019291, in part by the National Science Foundation (at Binghamton University) under Award PHY-2010365, in part by the US Air Force Office of Scientific Research (at Binghamton University) under Award FA9550-18-1-0223, and in part by the US Department of Energy, Office of Science, Office of Basic Energy Sciences (at SLAC National Accelerator Laboratory), under Contract DE-AC02-76SF00515. *(Corresponding author: Michael Chini.)*

Tran-Chau Truong, Christopher Lantigua, and Michael Chini are with the University of Central Florida, Orlando, FL 32816 USA (e-mail: chau.truong@ucf.edu; christopher.lantigua@ucf.edu; michael.chini@ucf.edu).

Yuxuan Zhang, Jack W. Agnes, and Bonggu Shim are with the Binghamton University, Binghamton, NY 13902 USA (e-mail: yzhan340@binghamton.edu; jagnes1@binghamton.edu; bshim@binghamton.edu).

Ruaridh Forbes is with the SLAC National Accelerator Laboratory, Menlo Park, CA 94025 USA (e-mail: ruforbes@slac.stanford.edu).

Color versions of one or more figures in this article are available at https://doi.org/10.1109/JSTQE.2024.3401689.

Digital Object Identifier 10.1109/JSTQE.2024.3401689

correlation is expressed as $hv = I_p + 3.17U_p$, where hv represents the maximum photon energy produced, I_p denotes the ionization potential of the medium involved in generation, and U_p is the ponderomotive energy. The latter is influenced by both laser intensity and the square of the driving wavelength [16], [2].

In recent years diode-pumped Ytterbium (Yb)-based laser systems have become increasingly prevalent in ultrafast science due to their femtosecond pulse durations and ability to run at very high repetition rates [17], [18]. However, a significant drawback compared to Ti-Sapphire laser systems is the ability to generate large bandwidths, due to constraints of the gain medium, which has typically capped pulse durations at greater than several hundred femtoseconds. To exploit the advantages of these systems for HHG and attosecond science experiments significant amounts of nonlinear compression is required to generate the prerequisite few-cycle laser fields. The use of stretched HCFs to construct long (>5 m) fiber systems [19] as well as multiple stages of compression [20], [21] have been used to provide the required amounts of broadening.

An attractive alternative to provide the levels of broadening needed to generate large bandwidth from the relatively long few-hundred femtosecond pulses from Yb laser systems is to exchange the gas medium in the HCF from atomic to molecular gases [22]. Due to the presence of both vibrational and rotational degrees of freedom there exists "delayed" nonlinear responses linked to field-induced alignment and stretching of the molecular bonds [23], [24]. Additionally, there are four-wave mixing processes connected to Raman transitions [25], [26]. For the typical pulse durations produced from Ti-Sapphire lasers these delayed nonlinear responses have a minimal impact [27] but this is not the case for the longer pulse durations produced from Yb lasers [28]. This increased rotational nonlinearity can be approximated as nearly instantaneous, leading to a time-dependent rotational nonlinear response which is present along with the electronic Kerr nonlinearity. Selecting the molecular gas based on the input pulse duration allows for a more than tenfold enhancement in total nonlinearity compared to an atomic gas with comparable nonlinear susceptibility and ionization potential [28].

In recent years studies have explored multiple aspects of molecular gas broadening including using frequency shifting of the pulses using stimulated Raman scattering (SRS) [29], [30], [31], [32], [33], [34], [35], [36] scaling to higher pulse energies [37] as well as higher repetition rates [38], [39]. Recent works have also explored the use of multiple pulses to exploit the use of pre-aligned molecules for spectral broadening and wavelength shifting [40]. For applications in HHG the ability to exploit SRS for frequency shifting to the IR is particularly appealing due the associated enhancement of the maximum cut-off energy [41], [37]. Despite the huge promise of molecular gases for both SRS frequency shift and broadening there exists several technical challenges surrounding the scaling to high repetition rates due to thermal effects [38].

In this article we review the theory of nonlinear optics in molecular gases, showcase experimental and theoretical results on spectral broadening and frequency shifting in molecular gases. The time-frequency properties of red-shifted pulses from molecular gas are discussed in detail, two methods for pulse compression are demonstrated experimentally, and severe thermal effects at high repetition rates are described along with mitigation strategies. In particular, we demonstrate new results about the role played by thermal lensing in determining the fiber energy efficiency, along with a method of using mixed gases to assist in average power scaling. Finally, we discuss the prospects of broadening into the mid-IR.

II. Theory of Spectral Broadening in Molecular Gases

One can theoretically model the propagation of the laser electric field in a gas-filled HCF using the nonlinear envelope equation (NEE) with a modal expansion assuming cylindrical symmetry [42], [43], [44], [29]. The propagation equation is given as

$$\frac{\partial \widetilde{E_m}}{\partial z} = i\left[k_{z,m}(\omega) - \kappa(\omega) + i\beta_m\right]\widetilde{E_m} + \frac{i}{2k_{z,m}(\omega)}\frac{\omega^2}{c^2}\frac{\widetilde{P_{NL,m}}}{\epsilon_0} - \frac{1}{2k_{z,m}(\omega)}\frac{\omega}{c}\frac{\widetilde{J_m}}{\epsilon_0 c} - \frac{\widetilde{\alpha_{NL,m}}}{2}, \quad (1)$$

where each term given by $\tilde{X}$ is in the spectral domain and is linked to its time domain counterpart, X, by the Fourier transform. The spectral representation of these terms is decomposed into discrete modal components, $\widetilde{X_m}$, and are written as $\tilde{X} = \Sigma_m \widetilde{X_m} J_0(\gamma_m r/r_c)$, where $J_0(\gamma_m r/r_c)$ is the normalized zeroth-order Bessel function, γ_m is the mth root of zeroth-order Bessel function J_0 and r_c is the radius of the capillary. For instance, E is the electric field envelope written as $\tilde{E} = \Sigma_m \widetilde{E_m} J_0(\gamma_m r/r_c)$. $k_{z,m} = \sqrt{k^2(\omega) - k_{\perp,m}^2}$ is the wave number in the propagation direction, where $k(\omega) = n(\omega)\omega/c$, $n(\omega)$ is the gas refractive index, ω is the angular frequency, c is the speed of light and $k_{\perp,m} = \gamma_m / r_c$ is the modal transverse wave number. $\kappa(\omega) = k_0 + (\omega - \omega_0)/v_g$, where ω_0 is the central frequency of the laser, and v_g is the group velocity of the fundamental mode ($v_g = (dk_{z,1}/d\omega|_{\omega=\omega_0})^{-1}$). Equation (1) is solved in the frame of the group velocity of the fundamental mode. The loss coefficient is given by $\beta_m = [0.5(1 + n_{cl}^2)/(n_{cl}^2 - 1)^{1/2}] (\gamma_m/k(\omega))^2/r_c^3$, where n_{cl} is the refractive index of cladding. P_{NL} is the nonlinear polarization which is given by $P_{NL}(t) = 2\epsilon_0 n_0 (n_2 I(t) + n_{Ram})E(t)$. Here ϵ_0 is the free space permittivity, n_0 is the linear refractive index, n_2 is the instantaneous nonlinear index coefficient, $I(t)$ is the intensity of the laser pulse and n_{Ram} is the index change due to the rotational Raman effect, which is described below. The plasma effects such as plasma defocusing and absorption are incorporated by calculating the free charge-induced current J which is written as $J(t) = (e^2/m_e)(\nu_e + i\omega)/(\nu_e^2 + \omega^2)\rho(t)E(t)$, where e and m_e are the electron charge and mass, respectively, ν_e is the electron collision frequency, and ρ is the free electron density. In addition,

$\alpha_{NL}(t) = \frac{\rho_0 W(I) I_p}{I} E(t)$ is the absorption due to optical field ionization (OFI), where ρ_0 is the neutral gas density, $W(I)$ is the OFI rate, and I_p is the ionization energy. The electric field propagation (1) is coupled with the plasma equation which is given by

$$\frac{\partial \rho}{\partial t} = W(I)(\rho_0 - \rho) - \frac{\rho}{\tau_r}, \tag{2}$$

where τ_r is the electron recombination time. Here, the first term on the right side describes plasma generation via the Perelemov-Popov-Terentev (PPT) OFI model [45], which incorporates both multiphoton and tunneling ionization, and the second term is about plasma recombination.

The nonlinear index change due to the rotational Raman effect is calculated via the quantum mechanical density matrix method [46], [47], [48], which is given as

$$n_{Ram} = -\frac{16\pi^2 N(\Delta\alpha)^2}{15\hbar n_0 c} \sum_l \frac{l(l-1)}{2l-1} \left(\frac{\rho_l}{2l+1} - \frac{\rho_{l-2}}{2l-3} \right) Im\left(e^{i\omega_{Ram} t} \int_{-\infty}^{t} I(t') e^{-i\omega_{Ram} t'} dt' \right), \tag{3}$$

where N is the gas number density, $\Delta\alpha$ is the polarizability anisotropy of the linear molecule, $\hbar$ is the reduced Plank's constant, $I(t')$ is the laser intensity, $\omega_{Ram} = 4\pi cR(2l-1)$ is the Raman angular frequency of the molecule, R is the rotational constant (for instance, 0.3902 cm^{-1} for CO_2 and 0.41 cm^{-1} for N_2O [49]), and ρ_l is the density matrix for the unperturbed molecular system given by

$$\rho_l = \frac{S_l (2l+1) e^{\frac{-hcRl(l+1)}{k_B T}}}{\sum_g S_g (2g+1) e^{\frac{-hcRg(g+1)}{k_B T}}} \tag{4}$$

where S_l is a statistical weighting factor (1 for both CO_2 and N_2O), h is Plank's constant, k_B is Boltzmann's constant, and T is the ambient temperature. Here we ignore the damping/dephasing factor because of its long timescale (tens of picoseconds). In our calculation, we use $\Delta\alpha = 16.3 \times 10^{-25}$ cm^3 for CO_2 and 22.7×10^{-25} cm^3 for N_2O, which are the measured values [47] by the state-of-the-art single-shot frequency domain holography technique [50], [51]. The information of parameters used in the simulation is shown in Table I for different gases.

Using the above approach, we perform simulations of spectral broadening in Ar, CO_2 and N_2O gases. For the simulations, the HCF has a length of 3.5 m and a radius of 250 μm. The input beam is a spatio-temporal Gaussian, and its focal spot size radius at the HCF entrance is 0.645 times the capillary radius for optimal coupling efficiency [52]. Fig. 1 shows (a, c, e) the on-axis (r = 0) spectra as a function of propagation distance and (b, d, f) the on-axis spectrum at the output of a HCF filled with each gas at 4.4 bars. Here we use laser pulses with a central wavelength (λ) of 1025 nm and pulse duration (τ) of 280 fs, and the input peak intensity (I) is 2×10^{12} W/cm^2. Since the information on dispersion for N_2O is lacking, the dispersion properties of N_2 are used for the N_2O calculation. As shown,

TABLE I
NUMERICAL PARAMETERS USED IN THE SIMULATIONS

Density Matrix Model Simulations					
	Ar	**N_2**	**O_2**	**N_2O**	**CO_2**
n_2 (x 10^{-19} cm^2/W)	1	0.74	0.95	2.1	1.3
R (cm^{-1})	N/A	2	1.44	0.41	0.3902
$\Delta\alpha$ (10^{-25} cm^3)	N/A	9.3	10.2	22.7	16.3
S_{even}	N/A	6	6	1	1
S_{odd}	N/A	3	3	1	1
Capillary Propagation simulations (3.5 m length)					
Capillary radius (a_0)	250 µm				
Input beam radius	0.645 a_0				
Pressure (bar)	4.4				
Peak Intensity (TW/cm^2)	2				
	Ar	**N_2**	**O_2**	**N_2O**	**CO_2**
Pulse duration (fs)	280	60	150	280	280
λ (µm)	1.025	2.4	4.1	1.025	1.025
Ionization energy (eV)	15.76	15.576	12.063	12.89	13.78

the spectral red shift from molecular gases is dominant due to the strong rotational Raman effect, while the spectrum from Ar gas is symmetric around the center wavelength due to the electronic Kerr nonlinearity alone. Due to the greater Raman effect for N_2O, spectral broadening is larger than that from Ar and CO_2. This can be understood by comparing the value of nonlinear index n_2 and the polarizability anisotropy $\Delta\alpha$ of each gas shown in Table I, where Ar has a small n_2, and both values $\Delta\alpha$ and n_2 of N_2O are larger than the ones of CO_2.

The difference in the characteristics of output spectra between molecular and atomic noble gases is clearly visible in the time-frequency spectrograms in Fig. 2(b) and (d). While the output pulses from Ar gas mainly exhibit positive chirp near the peak of the pulse intensity profile, the pulses from N_2O gas display both negative and positive chirp components, with a predominance of negative chirp at the leading edge of the pulse. This suggests that both normal dispersion from bulk materials and negatively-dispersive chirped mirrors could be used for pulse compression in different temporal regions of the pulse, which will be discussed in more detail in the following sections.

III. COMPRESSION OF FEW-CYCLE PULSES

The theoretical simulations of spectral broadening in molecular gas-filled HCFs highlight the potential benefits of rotational nonlinearity for realizing large spectral bandwidths and large compression factors from few-hundred femtosecond laser pulse durations. This enhancement has also been realized experimentally [29]. Fig. 3 shows the experimental results of pressure-dependent spectra measured in Ar, N_2 and N_2O-filled HCF, also with 250 μm radius and 3.5 m length. The driving laser pulses were obtained from a commercial Yb:KGW amplifier (Light Conversion PHAROS) with central wavelength of 1025 nm, pulse duration of 280 fs, energy of 400 μJ, and tunable repetition rate up to 50 kHz. For the results in Figs. 3 and 7, a reduced repetition rate of 250 Hz was used to eliminate the potential for multi-pulse interaction effects. As clearly seen in

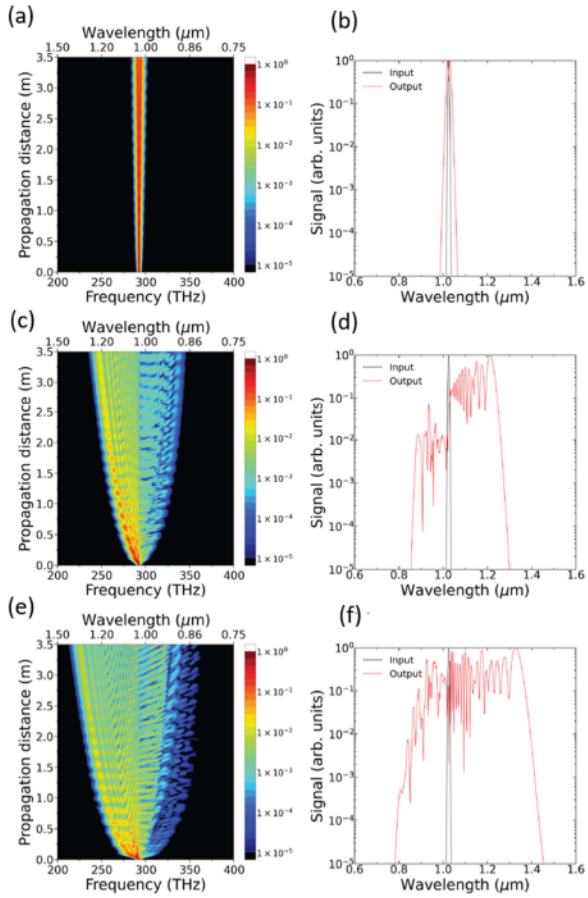

Fig. 1. Calculated spectral broadening in 4.4 bar Ar (a)-(b), CO_2 (c)-(d), N_2O (e)-(f) filled capillary with 3.5 m length and 250 μm radius: (a), (c), (e) On-axis (r = 0) spectra vs. distance and (b), (d), (f) output spectrum. The black line shows the input laser spectrum. The laser has a central wavelength of 1025 nm and 280 fs pulse duration, and its input peak intensity is 2×10^{12} W/cm^2.

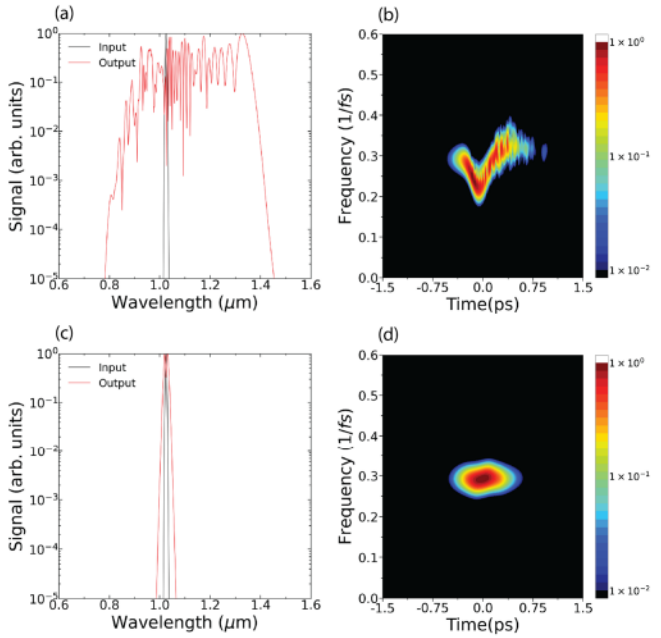

Fig. 2. Calculated (a) output spectra (red line) and (b) time-frequency analysis of the output spectra for N_2O at 4.4 bars. Calculated (c) output spectra (red line) and (d) time-frequency analysis of the output spectra for Ar at 4.4 bars. For both cases, the gas-filled capillary is 3.5 m long and its radius is 250 μm. The laser has a central wavelength of 1025 nm and 280 fs pulse duration, and its input peak intensity is 2×10^{12} W/cm^2.

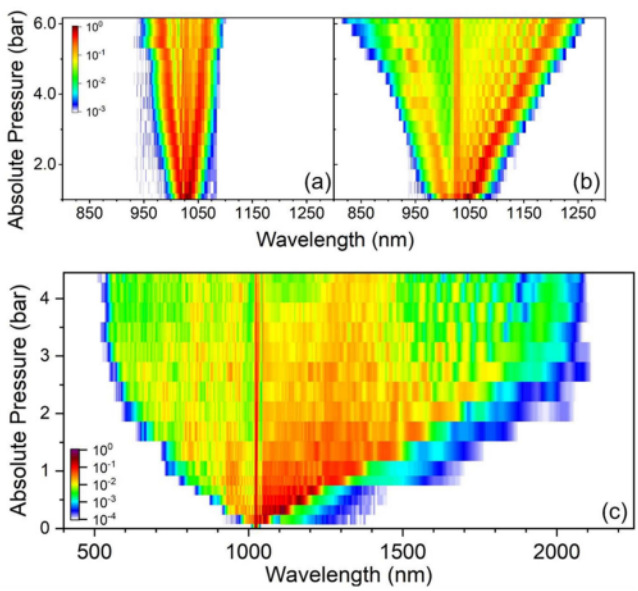

Fig. 3. Spectral broadening of (a) Ar, (b) N_2 and (c) N_2O at different static pressures. *(Reprinted with permission from [29] © The Authors, some rights reserved; exclusive licensee AAAS. Distributed under a CC BY-NC 4.0 License).*

Fig. 3(a) and (b), the spectrum obtained from N_2 is substantially broader than and red-shifted in comparison to that from Ar at the same pressure, in spite of the fact that both have similar electronic nonlinearity n_2 and ionization potential I_p. For N_2O, which has larger electronic and rotational nonlinearity than N_2, an even more substantial broadening and red-shifting is observed, resulting in a supercontinuum spectrum covering more than two octaves. The broad spectrum from N_2 gas was observed independently by other groups [31], [53], where the asymmetric, broad spectrum is attributed to the cascaded SRS and the excitation of high-order modes in the fiber propagation.

A. *Nonlinear Compression With Chirped Mirrors*

Aside from the generation of a broadband spectrum, the compression of few-cycle pulses further requires the compensation of the frequency chirp accumulated during nonlinear propagation. For N_2, the electronic and rotational nonlinearity are comparable, and the most energetic portion of the output pulse is expected to have a positive linear chirp for the laser parameters used in our experiment. As a result, the spectral phase resulting from propagation an N_2-filled HCF can be best compensated using chirped mirrors with negative group delay dispersion. As demonstrated in [29], a set of 8 pairs of complimentary-pair chirped mirrors (Ultrafast Innovations, PC1632) with spectral range of 700–1400 nm and nominal GDD of -85 fs^2/pair were used to compensate the dispersion of the relatively narrower spectrum generated with 6.5 bar N_2. The optimal compression was achieved when adding 20 mm CaF_2 and characterized by

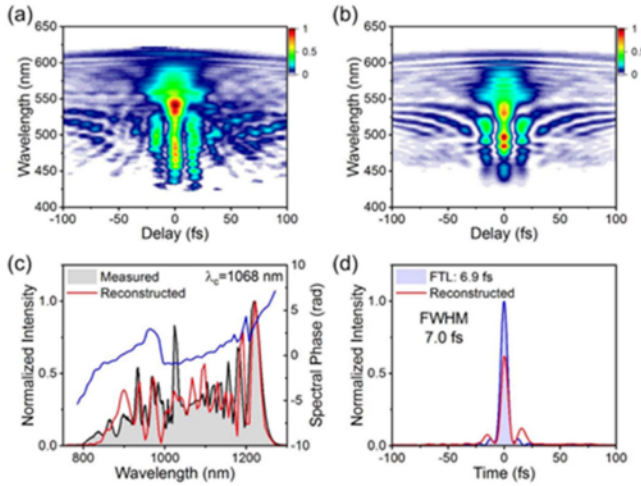

Fig. 4. SHG FROG characterization for compressed pulses from 6.5 bar N_2-filled in HCF and chirped mirrors. Measured (a) and reconstructed (b) traces. (c) Measured (grey), reconstructed (red) spectrum and spectral phase (blue). (d) Retrieved temporal intensity (red) and FTL intensity (blue). *(Reprinted with permission from [29] © The Authors, some rights reserved; exclusive licensee AAAS. Distributed under a CC BY-NC 4.0 License).*

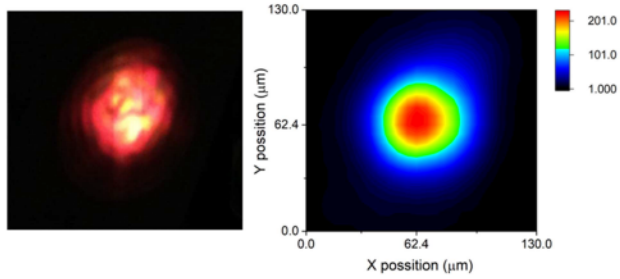

Fig. 5. Beam profiles after N_2O-filled capillary fiber taken by silicon-based cameras before (left) and after (right) a long pass filter cutting off at 1340 nm and a 73 μm thick silicon window. The left image shows visible and near-infrared light scattered by a card. The right image shows a representation of the beam profile through two-photon absorption in the camera sensor.

a home-built second harmonic generation frequency resolved optical gating (SHG FROG) device. As shown in Fig. 4, the compressed pulses with full-width at half-maximum (FWHM) duration of 7.0 fs are close to Fourier transform-limited (FTL) pulse duration of 6.9 fs. In other words, the combined electronic and rotational nonlinearities of N_2 enable the generation of a sub-two-cycle laser source with a large compression ratio of ~40 times.

B. Nonlinear Compression With Bulk Materials

A notable characteristic of spectral broadening from larger molecules such as CO_2 and N_2O is the heavy redshifted spectrum, which has the potential for generating long-wavelength few-cycle sources. This long wavelength side results from the interplay between the timescales associated with the molecular rotational nonlinearity and the duration of the driving pulse. The leading edge of the laser pulse initiates the electronic response, which is then amplified by the alignment of the molecules, such that the instantaneous frequency continues to shift towards the red wavelengths even during the central part of the temporal intensity profile. As a result, the long wavelength side of the broadened spectrum possesses an overall negative temporal chirp, which suggests an alternative approach to post compression in molecular gases, using the normal dispersion of bulk materials. This interesting feature of molecular gases was first observed by Safaei and co-workers, who lengthen 40 fs pulses from Ti: Sapphire amplifier to ~700 fs positively-chirped pulses in order to take advantage of rotational broadening of N_2 gas filled in a HCF, and then employed the normal dispersion of fused silica (FS) to compress the negatively-chirped, spectrally broadened output pulses to <11 fs, [31]. The observation of negatively-chirped output pulses was dubbed multidimensional solitary states (MDSS), since the pulse compression due to the Raman effect was accompanied by a smaller effective mode radius in the HCF, due to coupling to higher-order modes. Red-shifted supercontinuum spectra have now been obtained using few-hundred femtosecond sources with NIR central wavelengths of 1030 nm [29], [53] 780 nm [31] and even visible central wavelength of 400 nm [54]. Furthermore, the generated long-wavelength spectra from molecular gas-filled HCFs have been experimentally shown to produce high-order harmonics with higher cut-off photon energy than self-phase modulation-based sources [41] and with continuous spectra that suggest sub-cycle gating of the HHG process.

The short wavelength (<1000 nm in our experiments) light generated in molecular gas-filled HCFs has been observed to have an unstable, multi-mode beam profile, as shown in Fig. 5. On the other hand, the long wavelength (1340–2000 nm) side of the spectrum, which can be selected by spectral filtering with a long-pass filter and a thin Si window at Brewster's angle, has a clean and stable beam profile (Fig. 5(b)). This behavior was also observed in N_2 gas-filled HCFs and was attributed to intermodal interactions during the formation of MDSS [31]. Both the spectral broadening and the evolution of these modes occurs primarily near the beginning of the fiber, which can potentially allow the reduction of the conventional fiber length used for SPM.

An experimental setup was implemented to investigate the use of bulk materials to compress the red-shifted supercontinuum resulting from broadening of a Yb-doped amplifier in N_2O gas [55]. In the experiments, we achieved a broad spectrum by propagating 280 fs, 400 μJ pulses through a HCF, with radius of 200 μm and length of 1.4 m, and filled with 2.7 bar of N_2O. Subsequently, the generated supercontinuum beam was transmitted through 4 mm NaCl windows, taking advantage of the normal dispersion of NaCl in the short-wave infrared, to compress the pulses enroute to the SHG-FROG setup used for pulse characterization. As expected, the FROG results shown in Fig. 6 reveal that the pulses were compressed to an impressive 11.5 fs pulse duration, 175 μJ pulse energy, equivalent to less than 3 cycles at the central wavelength of ~1200 nm. The compressed pulse durations observed here with N_2O and bulk compression are comparable to those previously observed with Xe gas and chirped mirror at 1030 nm [56], [57] and also with

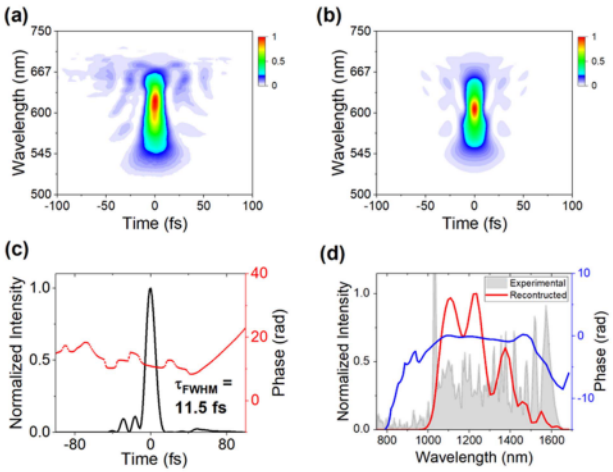

Fig. 6. SHG FROG characterization of bulk compression using NaCl. Measured (a) and reconstructed (b) traces. (c) Retrieved temporal intensity (black) and phase (red). (d) Measured (grey), reconstructed (red) spectrum and spectral phase (blue).

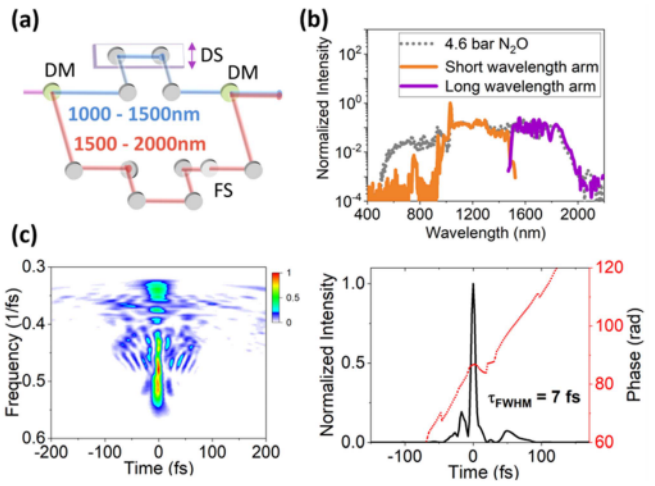

Fig. 7. (a) Light-field synthesizer setup from HCF filled with N_2O gas, DM, dichroic mirror; DS, delay stage; FS, fused silica. (b) Output spectrum from HCF (grey), spectrum of short- (orange) and long- (purple) wavelength arm of synthesizer. (c) Left: measured FROG trace of synthesizer pulses; Right: retrieved temporal intensity (black) and spectral phase (red). *(Adapted with permission from [59] © Optical Society of America).*

vibrationally-excited H_2 gas and silica glass compression at 1800 nm [58], which yielded sub-three-cycle pulses but with lower pulse energy and in a more complex setup. Despite the generated spectrum spanning from 800 nm to 1650 nm, the spectral range of the FROG trace in Fig. 6(a) and the retrieved spectrum in Fig. 6(d) indicates that only the longer-wavelength (above 1 micron) side of the spectrum contributes to the short pulses. This is because the long wavelength range inherits the negative dispersion from the rotational nonlinearity and therefore is compressed by normal dispersion of the bulk materials. Furthermore, due to the limitation of the temporal window of the single-shot geometry and the difficulty of resolving low signal levels associated with the much lower-intensity, uncompressed pulses, the short-wavelength component can't be seen in the FROG trace. In sum, these observations align with our simulations and highlight the distinctive negative chirp in the long-wavelength spectrum generated from molecular gases.

Increasing the static pressure to 4.6 bar N_2O allows the extension of the long-wavelength side of the spectrum up to $\sim 2\ \mu$m wavelength and enables further pulse compression by using only bulk materials. However, the third-order dispersion presents a significant limitation when using the dispersion of a single material for pulse compression. The experimental results in [59], on the other hand, showed that sub-two-cycle pulses can be obtained by a simple, off-the-shelf light field synthesizer in which the broad output spectrum split into two arms of Mach-Zehnder interferometer, separately compressed, and then recombined by a pair of dichroic mirrors with cutoff wavelength near 1500 nm, as shown in Fig. 7(a) and (b). While the short wavelength arm is compressed to 12.5 fs pulse duration (<3.5 optical cycles at the central wavelength of 1170 nm) using the normal dispersion of CaF_2 and fused silica optics in the beam path, the long-wavelength arm is compressed to 22.2 fs pulse duration (4 optical cycles at the central wavelength of 1690 nm) by the anomalous dispersion of fused silica. As seen in Fig. 7(c), the final synthesized pulses with 7 fs pulse duration (1.5 optical cycles) and red-shifted central wavelength of 1364 nm are generated in a relatively simple and inexpensive setup. The overall energy efficiency of the setup, with 11% of the driving laser pulse energy in the final compressed pulses, is comparable to that of optical parametric amplification (OPA) and optical parametric chirped-pulse amplification (OPCPA) systems, but with a broader spectrum that is not limited by the phase matching of nonlinear crystals.

IV. Thermal Effects and Power Scaling

A. Thermal Effects

The theoretical results described in Section II consider the interaction of a single pulse with the molecular gas-filled fiber, while the experiments described in Section III were performed with a relatively low repetition rate of 250 Hz. At higher repetition rates, thermal effects in HCFs limit both the spectral broadening and the throughput efficiency of the fiber. These thermal effects are present in both atomic and molecular gas systems to different degrees.

In atomic gases, it has been shown that photoionization and heating of the fiber walls due to absorption causes a reduction in throughput power when attempting to scale pulse compression systems to >100 W average power levels [60]. Additionally, at high repetition rates, gas density depressions can form inside the fiber due to ionization-induced heating, which alter the refractive index of the medium on millisecond time scales [61], [62]. Lensing by the gas density depressions causes a defocusing of the beam that negatively impacts the spectral bandwidth of the generated supercontinuum.

Thermal effects due to repeated laser interactions are present in molecular gases as well. However, these effects occur at much lower average powers, and are the result primarily of thermal excitation of rotational and vibration degrees of freedom that act

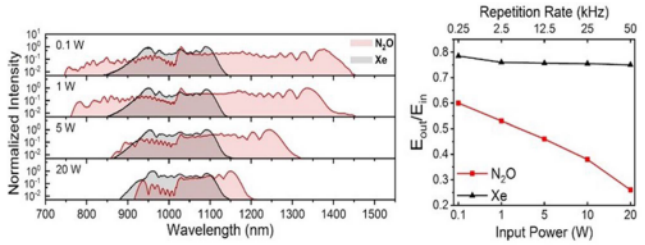

Fig. 8. Power-dependent spectral broadening (a) and throughput (b) of 1 bar N_2O vs 1.6 bar Xe gases filled in a 3.5 m long, 200 μm core radius HCF. *(Reprinted with permission from* [38] *© Optical Society of America).*

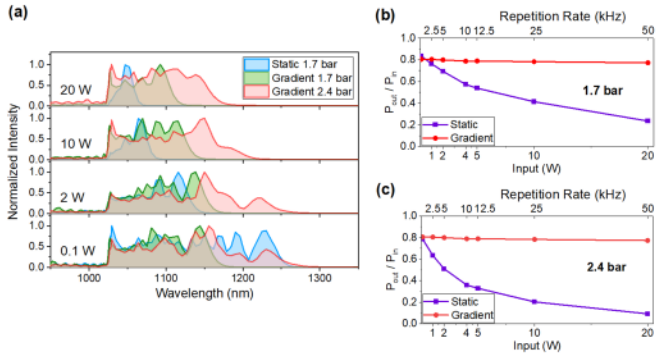

Fig. 9. Spectral broadening (a) and power transmitted (b)-(c) from 1.7 bar and 2.4 bar N_2O filled in a HCF in static and gradient pressure configurations.

to reduce the spectral bandwidth and throughput efficiency of the fiber. In molecular gases, the nonlinear response is enhanced due to the alignment of the molecules with the electric field of the laser pulse. However, at high average powers the molecules continue to be excited to higher rotational and vibrational levels, which reduces the rotational coherence with the laser pulses, and affects the enhanced nonlinearity. This spectral narrowing in molecular gas-filled HCFs at high average powers is clearly illustrated in Fig. 8, where the spectral bandwidth obtained from an N_2O-filled fiber is compared with a xenon-filled fiber for various input average powers, with a fixed pulse energy and variable repetition rate. As the repetition rate of the source increases, the spectral bandwidth of N_2O decreases, while that of xenon stays relatively constant over this range of input powers.

In addition to a reduction in the spectral bandwidth, Fig. 8 also illustrates a drop in the throughput efficiency of N_2O-filled HCF compared to xenon. At the highest measured input power, 20W, the throughput of the N_2O filled HCF drops to 20%. One of reasons is from the fundamental limitation associated with red-shifted spectra: even if 100% photon-to-photon conversion efficiency is achieved, the overall pulse energy would be reduced according to the shift of the spectral weight to lower photon energies. Moreover, molecular gases experience a thermal lensing effect due to a non-uniform density distribution of the gas inside the fiber. The molecules near the core of the beam experience the highest rotational temperature. This rotational kinetic energy is then transferred to translational energy via molecular collisions, resulting in the increase of linear velocity, followed by the appearance of a lower density region at the core and a higher density of gas molecules in the outer regions of the beam. This creates a negative lens, with a higher refractive index near the edges of the beam and a lower refractive index in the center. This negative lens defocuses the incoming beam, which negatively impacts the coupling efficiency into the fiber, causes coupling into higher-order modes, and thus reduces the overall throughput efficiency. This thermal lensing effect becomes more dramatic as the average power sent into the fiber is increased. In contrast, atomic gases have more well-behaved nonlinearity, and the fiber coupling efficiency is mainly reduced only by ionization, which is kept to a minimum in the experiments, resulting in its high output power.

The reduction in throughput efficiency and spectral narrowing observed in molecular gases limits their applicability for high-power systems. However, various mitigation techniques and strategies have been explored that give promising results and offer the possibility to scale molecular gas filled HCFs to higher average power levels.

B. Pressure Gradient

One method to alleviate the thermal effects associated with molecular gases is to utilize a pressure gradient between the entrance and exit tubes of the fiber. This approach was previously used to increase the input power and pulse energy for pulse compression using noble gas filled HCFs [62], [11]. In the experiment detailed in this paper, a pressure gradient is established along a 1-meter HCF with a 375 μm core radius. The fiber is filled with N_2O at the exit, and the entrance of the fiber is held under vacuum conditions. The impact of the pressure gradient scheme can be seen in Fig. 9, where the results of spectral broadening and throughput efficiency are compared to a static pressure configuration. From the Fig. 9(b) and (c), it can be seen that the power throughput in the static pressure configuration drops significantly from 80% to 30% as repetition rate of the input to the HCF is increased from 0.25 kHz to 50 kHz. In comparison, the results obtained under the pressure gradient scheme, with a backing pressure of 1.7 and 2.4 bar, shows a nearly constant 80% throughput efficiency as the average power input sent into the fiber increases. This is because the pressure gradient inside the fiber suppresses the effects of thermal lensing by essentially maintaining a vacuum at the entrance of the fiber, thereby avoiding the effects of negative lensing, and thus stabilizing the beam coupling into the fiber. As seen in Fig. 9(a), the spectral bandwidth obtained from the 1.7 bar gradient pressures (green line) is less affected by increases in the average power when compared to the significant spectral narrowing seen at the static (blue line). In this case, the reduced number of molecules interacting with laser can be a reason for the spectral narrowing. To examine how thermal effects impact the spectrum, the pressure gradient with the same quantity of molecular gas in fibers was chosen. In Fig. 9(a) we additionally show the spectra corresponding to a 2.4 bar gradient (red line), which has the same spectral bandwidth as the static pressure of 1.7 bar at low power (0.1 W). While broader bandwidths can

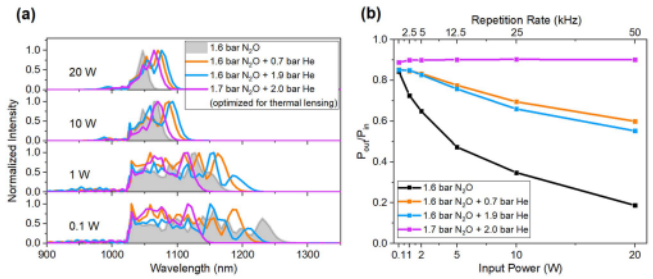

Fig. 10. Power transmitted (a) and spectral broadening (b) of N_2O mixed with helium gas filled in a HCF at different configurations.

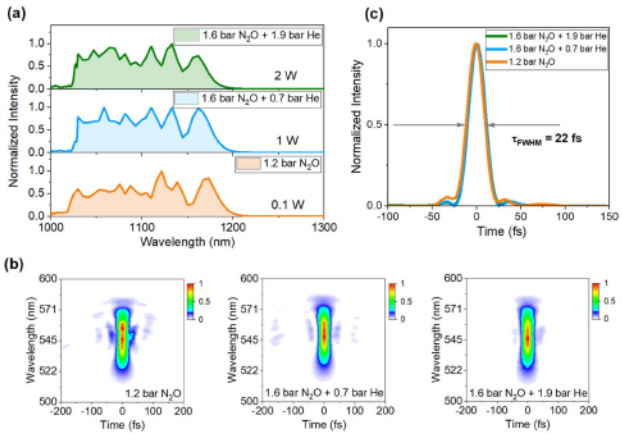

Fig. 11. Measured spectra (a), SHG-FROG traces (b) and retrieved temporal intensities (c) for different mixtures of N_2O and He gas.

be obtained at higher repetition rates than in the static pressure configuration, spectral narrowing is still present in the pressure gradient scheme.

Increasing the backing pressure can enhance the spectral bandwidth obtained from the HCF system, but as the pressure difference increases between the two sides, the flow rate of gas also increases. Beyond a critical pressure, that is dependent upon both the fiber and gas parameters, the gas flow transitions from a laminar to a turbulent regime, causing spatial instability in the beam profile [39], which limits the effectiveness of this scheme.

C. Mixed Gases

An alternate approach to mitigating the thermal effects involves a mixed gas medium that combines the molecular gas with a buffer gas [55], [63]. In this scheme, the buffer gas is expected to play a catalytic role in the cooling process by extracting rotational heat from the molecules and reducing the thermal lensing effect. A suitable buffer gas should therefore have good thermal conductivity, but also high ionization potential. Helium matches both these criteria, and a previous study also observed the effectiveness of helium in thermal mitigation in high-repetition rate photoionization of krypton gas [64]. To test its impact as a buffer gas in a molecular gas-filled HCFs, a 1-meter long HCF with a core radius of 375 um is filled with N_2O at a static pressure of approximately 1.6 bar, and then subsequently filled and mixed with varying pressures of helium. Fig. 10 displays the results of spectral broadening and throughput efficiency in a mixed gas system in contrast to just the molecular gas. In the pure N_2O configuration, the spectral narrowing and notable drop in throughput efficiency, from 85% to ~20% are seen as the input power to the HCF system is increased. When comparing the mixed gas scheme, the presence of helium improves both the spectral bandwidth and power throughput at high-average powers. This improvement is attributed to helium's role in removing heat from molecules, causing them to stay at lower rotational energy levels. As a result, the coherence between the molecules and the laser pulses is recovered, along with a reduction in thermal lensing. With helium and N_2O in a mixed gas scheme, the throughput efficiency can reach 90% depending on how gases, as seen in the pink line in Fig. 10(b). In this scenario, the mixed gas scheme was optimized to maximize the throughput efficiency of the HCF. The immiscibility of He and molecular gas leads to long-lived local distributions of gases in the fiber system [65], and the fiber can be configured such that a boundary exists between He and N_2O. Here, filling the fiber so that the boundary of immiscibility exists just beyond the entrance allows the fiber to be configured such that the entrance of the fiber is mostly He and the remaining portion of the fiber being mostly N_2O. The effect of this is an improvement in the throughput efficiency of the fiber. Helium is less susceptible to heating at higher repetition rates compared to N_2O, and thus the impact of thermal lensing is reduced thereby improving the coupling efficiency into the fiber and improving the throughput efficiency overall. This of course comes at the expense of spectral broadening because the laser pulses have a smaller interaction length with N_2O, which can be seen in the pink line spectrum of Fig. 10(a). However, the ability to tune and optimize the configuration of the fiber in a mixed gas scheme is a promising feature of the scheme.

While different amounts of buffer gas can be used to mitigate the thermal effects of molecular gas, the properties of the generated supercontinuum spectra for pulse compression need to be considered. Spectral broadening associated with N_2O leads to the generation of MDSS that are characterized by negative chirps, which can be compensated for by the normal dispersion of optical materials. To ensure that the addition of helium does not impact the generation of MDSS, two different gas mixtures from the previous experiment with similar spectra, but at different repetition rates were chosen to compare with the post compression of pure N_2O as shown in Fig. 11(a). The spectra all supported a transform-limited pulse duration of approximately 20 fs as shown in Fig. 11(b), and in each case an identical thickness of glass was used for pulse compression. Fig. 11(c) shows the results obtained from SHG-FROG measurements under each of the three conditions. The retrieved FROG traces are nearly identical, each corresponding to a compressed pulse duration of approximately 22 fs. These results demonstrate that the inclusion of helium as a buffer gas inside the fiber does not impact the generation of the MDSS.

V. Prospects for Few-Cycle Mid-IR Pulses

When driven by lasers with central wavelength in the near-infrared, the above results show promising opportunities for

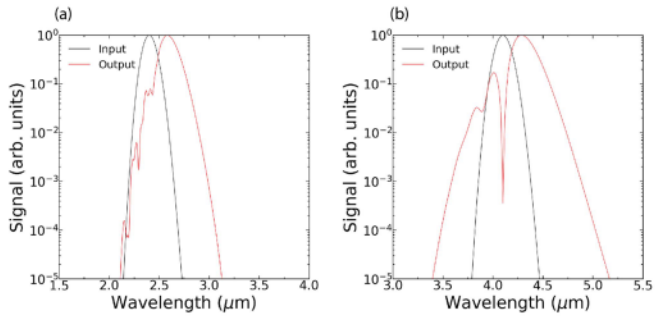

Fig. 12. Calculated output spectra (red line) for (a) N_2 at 4.4 bars with a laser pulse of $\lambda = 2400$ nm, $\tau = 60$ fs, and $I = 2 \times 10^{12}$ W/cm^2 and (b) O_2 at 4.4 bars with a laser pulse of $\lambda = 4100$ nm, $\tau = 150$ fs, and $I = 2 \times 10^{12}$ W/cm^2. The gas-filled capillary is 3.5 m long and its radius is 250 μm.

producing longer-wavelength, few-cycle pulses, which have clear applications to HHG and attosecond pulse generation. One attractive prospect, then, is to use longer-wavelength driving lasers to further push the central wavelength into the mid-infrared, where few-cycle driving lasers can potentially generate attosecond pulses with photon energies extending beyond 1 keV [66]. Of these, driving lasers based on Tm-doped fiber [67] or solid-state [68] gain media, as well as Cr- [69], [70] and Fe-doped [71] ZnSe are especially attractive due to their femtosecond pulse durations and multi-millijoule pulse energies.

To explore the potential of these lasers for driving SRS-enhanced spectral broadening, we perform simulations using laser pulses with longer wavelengths and different gas molecules. In particular, we focus on the wavelengths and pulse durations of existing Cr:ZnSe and Fe:ZnSe amplifiers, and on N_2 and O_2 gases which are minimally absorbing in the mid-infrared. Again, the capillary length is chosen to be 3.5 m and its radius is 250 μm. Fig. 12 shows the output spectra for (a) N_2 at 4.4 bars when a laser pulse with $\lambda = 2400$ nm, $\tau = 60$ fs, and $I = 2 \times 10^{12}$ W/cm^2 interacts with the N_2 filled capillary, and (b) O_2 at 4.4 bars when a laser pulse with $\lambda = 4100$ nm, $\tau = 150$ fs, and $I = 2 \times 10^{12}$ W/cm^2 interacts with the O_2 filled capillary. Overall, spectral broadening is reduced in comparison with that from N_2O and CO_2 because of the smaller rotational Raman effects in N_2 and O_2. Furthermore, spectral broadening from O_2 is more symmetric compared with dominant red-shifts from N_2. This is due to greater plasma generation, resulting in larger blue shift in O_2 because of its smaller ionization energy (12.063 eV for O_2 and 15.576 eV for N_2).

VI. Conclusion

In conclusion, molecular gas-filled HCFs offer a promising platform for the generation of few-cycle pulses in spectral regions which are inaccessible using standard laser gain media. In particular, the use of molecules with large rotational nonlinearity can allow the generation of strongly red-shifted few-cycle pulses, which are especially attractive for cutoff scaling of attosecond HHG sources. While peak and average power scaling of molecular gas-filled HCFs presents significant challenges, the potential for generating tunable few-cycle sources with substantially higher overall conversion efficiency than parametric amplifiers is a strong motivation for pursuing novel thermal energy reduction schemes.

Acknowledgment

Author Michael Chini acknowledges useful conversations with Yi Wu and Z. Alphonse Marra regarding the Cr:ZnSe and Fe:ZnSe laser parameters used in the simulations of Section VI.

References

[1] D. Strickland and G. Mourou, "Compression of amplified chirped optical pulses," *Opt. Commun.*, vol. 55, no. 6, pp. 447–449, 1985.
[2] T. Brabec and F. Krausz, "Intense few-cycle laser fields: Frontiers of nonlinear optics," *Rev. Mod. Phys.*, vol. 72, 2000, Art. no. 545.
[3] R. W. Boyd, *Nonlinear Optics*, 3rd. ed. New York, NY, USA: Academic, 2008.
[4] G. Cerullo et al., "Mirror-dispersion-controlled sub-10-fs optical parametric amplifier in the visible," *Opt. Lett.*, vol. 24, pp. 1529–1531, 1999.
[5] M. Nisoli, S. D. Silvestri, and O. Svelto, "Generation of high energy 10 fs pulses by a new pulse compression technique," *Appl. Phys. Lett.*, vol. 68, pp. 2793–2795, 1996.
[6] C. P. Hauri et al., "Generation of intense, carrier-envelope phase-locked few-cycle laser pulses through filamentation," *Appl. Phys. B*, vol. 79, pp. 673–677, 2004.
[7] C. P. Hauri et al., "Generation of intense few-cycle laser pulses through filamentation – parameter dependence," *Opt. Exp.*, vol. 13, pp. 7541–7547, 2005.
[8] F. Silva et al., "Multi-octave supercontinuum generation from mid-infrared filamentation in a bulk crystal," *Nature Commun.*, vol. 3, 2012, Art. no. 807.
[9] M. Seidel et al., "All solid-state spectral broadening: An average and peak power scalable method for compression of ultrashort pulses," *Opt. Exp.*, vol. 24, pp. 9412–9428, 2016.
[10] L. Gallmann et al., "Comparison of the filamentation and the hollow-core fiber characteristics for pulse compression into the few-cycle regime," *Appl. Phys. B*, vol. 86, pp. 561–566, 2007.
[11] A. Suda, M. Hatayama, K. Nagasaka, and K. Midorikawa, "Generation of sub-10-fs, 5-mJ-optical pulses using a hollow fiber with a pressure gradient," *Appl. Phys. Lett.*, vol. 86, 2005, Art. no. 111116.
[12] G. Fan et al., "70 mJ nonlinear compression and scaling route for an Yb amplifier using large-core hollow fibers," *Opt. Lett.*, vol. 46, pp. 896–899, 2021.
[13] T. Nagy, M. Forster, and P. Simon, "Flexible hollow fiber for pulse compressors," *Appl. Opt.*, vol. 47, no. 18, pp. 3264–3268, 2008.
[14] B. E. Schmidt et al., "CEP stable 1.6 cycle laser pulses at 1.8 μm," *Opt. Exp.*, vol. 19, pp. 6858–6864, 2011.
[15] G. Fan et al., "Hollow-core-waveguide compression of multi-millijoule CEP-stable 3.2 μm pulses," *Optica*, vol. 3, pp. 1308–1311, 2016.
[16] P. B. Corkum, "Plasma perspective on strong field multiphoton ionization," *Phys. Rev. Lett.*, vol. 71, pp. 1994–1997, 1993.
[17] C. R. E. Baer et al., "Femtosecond thin-disk laser with 141 W of average power," *Opt. Lett.*, vol. 35, pp. 2302–2304, 2010.
[18] S. Hädrich et al., "Energetic sub-2-cycle laser with 216 W average power," *Opt. Lett.*, vol. 41, pp. 4332–4335, 2016.
[19] Y.-G. Jeong et al., "Direct compression of 170-fs 50-cycle pulses down to 1.5 cycles with 70% transmission," *Sci. Rep.*, vol. 8, 2018, Art. no. 11794.
[20] J. Rothhardt et al., "53 W average power few-cycle fiber laser system generating soft x rays up to the water window," *Opt. Lett.*, vol. 39, pp. 5224–5227, 2014.
[21] L. Lavenu et al., "High-power two-cycle ultrafast source based on hybrid nonlinear compression," *Opt. Exp.*, vol. 27, pp. 1958–1967, 2019.
[22] E. Haddad et al., "Molecular gases for pulse compression in hollow core fibers," *Opt. Exp.*, vol. 26, pp. 25426–25436, 2018.
[23] A. Couairon and A. Mysyrowicz, "Femtosecond filamentation in transparent media," *Phys. Rep.*, vol. 441, pp. 47–189, 2007.
[24] O. Kwon et al., "Raman effect in the spectral broadening of ultrashort laser pulses in saturated versus unsaturated hydrocarbon molecules," *Opt. Exp.*, vol. 28, pp. 980–990, 2020.
[25] S. E. Harris and A. V. Sokolov, "Subfemtosecond pulse generation by molecular modulation," *Phys. Rev. Lett.*, vol. 81, pp. 2894–2897, 1998.

[26] A. V. Sokolov et al., "Raman generation by phased and antiphased molecular states," *Phys. Rev. Lett.*, vol. 85, pp. 562–565, 2000.
[27] A. M. Zheltikov, "Understanding the nonlinear phase and frequency shift of an ultrashort light pulse induced by an inertial third-order optical nonlinearity," *Phys. Rev. A*, vol. 79, 2009, Art. no. 023823.
[28] J. K. Wahlstrand, Y.-H. Cheng, and H. M. Milchberg, "Absolute measurement of the transient optical nonlinearity in N_2, O_2, N_2O, and Ar," *Phys. Rev. A*, vol. 85, 2012, Art. no. 043820.
[29] J. E. Beetar et al., "Multioctave supercontinuum generation and frequency conversion based on rotational nonlinearity," *Sci. Adv.*, vol. 6, 2020, Art. no. eabb5375.
[30] G. Fan et al., "High energy redshifted and enhanced spectral broadening by molecular alignment," *Opt. Lett.*, vol. 45, no. 11, pp. 3013–3016, 2020.
[31] R. Safaei et al., "High-energy multidimensional solitary states in hollow-core fibres," *Nature Photon.*, vol. 14, pp. 733–739, 2020.
[32] Y.-H. Chen and F. Wise, "Unified and vector theory of Raman scattering in gas-filled hollow-core fiber across temporal regimes," *APL Photon.*, vol. 9, no. 3, 2024, Art. no. 030902.
[33] S.-F. Gao et al., "From Raman frequency combs to supercontinuum generation in nitrogen-filled hollow-core anti-resonant fiber," *Laser Photon. Rev.*, vol. 16, Apr. 2022, Art. no. 2100426.
[34] M. Sabbah, F. Belli, C. Brahms, and J. C. Travers, "Effect of rotational Raman response on ultra-flat supercontinuum generation in gas-filled hollow-core photonic crystal fibers," *Opt. Exp.*, vol. 31, pp. 28273–28284, 2023.
[35] Y. P. Yatsenko, A. V. Gladyshev, and I. A. Bufetov, "Coherent mid-IR supercontinuum in a hollow core fiber filled with a mixture of deuterium and nitrogen," *Bull. Lebedev Phys. Inst.*, vol. 50, pp. S996–S1005, 2023.
[36] A. Gladyshev, Y. Yatsenko, A. Kolyadin, and I. Bufetov, "Visible to mid-infrared supercontinuum initiated by stimulated Raman scattering of 1.03 μm ultrashort pulses in a gas-filled silica fiber," *Photonics*, vol. 9, 2022, Art. no. 997.
[37] M. Dorner-Kirchner et al., "HHG at the carbon K-edge directly driven by SRS red-shifted pulses from an ytterbium amplifier," *Amer. Chem. Soc. Photon.*, vol. 10, no. 1, pp. 84–91, 2023.
[38] J. E. Beetar et al., "Thermal effects in molecular gas-filled hollow-core fibers," *Opt. Lett.*, vol. 46, no. 10, pp. 2437–2440, 2021.
[39] L. Arias et al., "Few-cycle Yb laser source at 20 kHz using multidimensional solitary states in hollow-core fibers," *Opt. Lett.*, vol. 47, no. 14, pp. 3612–3615, 2022.
[40] Z. Rodnova, T. Saule, G. Gibson, and C. A. Trallero-Herrero, "Molecular alignment-assisted spectral broadening and shifting in the near-infrared with a recycled depleted pump from an optical parametric amplifier," *Opt. Exp.*, vol. 31, no. 25, pp. 42327–42337, 2023.
[41] K. Légaré et al., "Raman red-shift compressor: A simple approach for scaling the high harmonic generation cut-off," *Adv. Photon. Res.*, vol. 2, no. 11, 2021, Art. no. 2100113.
[42] C. Courtois C et al., "Propagation of intense ultrashort laser pulses in a plasma filled capillary tube: Simulations and experiments," *Phys. Plasmas*, vol. 8, 2001, Art. no. 3445.
[43] M. Nurhuda et al., "Propagation dynamics of femtosecond laser pulses in a hollow fiber filled with argon: Constant gas pressure versus differential gas pressure," *J. Opt. Soc. Amer. B*, vol. 20, 2003, Art. no. 2002.
[44] X. Gao et al., "Ionization-assisted spatiotemporal localization in gas-filled capillaries," *Opt. Lett.*, vol. 43, 2018, Art. no. 3112.
[45] A. M. Perelomov, V. S. Popov, and M. V. Terent'ev, "Ionization of Atoms in an Alternating Electric Field," *J. Exp. Theor. Phys.*, vol. 50, 1966, Art. no. 1393.
[46] Y. Chen, S. Varma, A. York, and H. Milchberg, "Single-shot, space- and time-resolved measurement of rotational wavepacket revivals in H_2, D_2, N_2, O_2, and N_2O," *Opt. Exp.*, vol. 15, pp. 11341–11357, 2007.
[47] D. Dempsey et al., "Comparative study of optical nonlinearities of CO2 and NO2 via single-shot spatio-temporally-resolved visualization," *Opt. Commun.*, vol. 545, 2023, Art. no. 129669.
[48] J. K. Wahlstrand, Y. H. Cheng, and H. M. Milchberg, "Absolute measurement of the transient optical nonlinearity in N_2, O_2, N_2O, and Ar," *Phys. Rev. A*, vol. 85, 2012, Art. no. 043820.
[49] C. H. Lin et al., "Birefringence arising from the reorientation of the polarizability anisotropy of molecules in collisionless gases," *Phys. Rev. A*, vol. 13, 1976, Art. no. 813.
[50] S.P. Le Blanc et al., "Single-shot measurement of temporal phase shifts by frequency-domain holography," *Opt. Lett.*, vol. 25, pp. 764–766, 2000.
[51] D. Dempsey et al., "Single-shot ultrafast visualization and measurement of laser–matter interactions in flexible glass using frequency domain holography," *Opt. Lett.*, vol. 45, 2020, Art. no. 1252.
[52] M. Nisoli et al., "Toward a terawatt-scale sub-10-fs laser technology," *IEEE J. Sel. Topics Quantum Electron.*, vol. 4, no. 2, pp. 414–420, Mar./Apr. 1998.
[53] P. A. Carpeggiani et al., "Extreme Raman red shift: Ultrafast multimode nonlinear space-time dynamics, pulse compression, and broadly tunable frequency conversion," *Optica*, vol. 7, pp. 1349–1354, 2020.
[54] M. Kumar et al., "Generating ultrashort visible light pulses based on multidimensional solitary states in gas-filled hollow core fiber," *APL Photon.*, vol. 8, 2023, Art. no. 056104.
[55] T.-C. Truong, "Progress towards attosecond science with a turn-key industrial-grade ytterbium laser," Ph.D. dissertation, Phys. Dept., Univ. Central Florida, Orlando, FL, USA, 2023.
[56] J. E. Beetar et al., "Hollow-core fiber compression of a commercial Yb:KGW laser amplifier," *J. Opt. Soc. Amer. B*, vol. 36, pp. A33–A37, 2019.
[57] L. Losev et al., "Compression of few-microjoule femtosecond pulses in a hollow-core revolver fiber," *Fibers*, vol. 11, 2023, Art. no. 22.
[58] L. L. Losev, V. S. Pazyuk, and A. V. Gladyshev, "Femtosecond hydrogen Raman frequency-shifter/pulse-compressor based on revolver fiber," *IEEE J. Sel. Topics Quantum Electron.*, vol. 30, Nov./Dec. 2024, Art. no. 8700105.
[59] T.-C. Truong, J. E. Beetar, and M. Chini, "Light-field synthesizer based on multidimensional solitary states in hollow-core fibers," *Opt. Lett.*, vol. 48, pp. 2397–2400, 2023.
[60] N. Jhajj, Y.-H. Cheng, J. K. Wahlstrand, and H. M. Milchberg, "Optical beam dynamics in a gas repetitively heated by femtosecond filaments," *Opt. Exp.*, vol. 21, pp. 28980–28986, 2013.
[61] Y.-H. Cheng, J. K. Wahlstrand, N. Jhajj, and H. M. Milchberg, "The effect of long timescale gas dynamics on femtosecond filamentation," *Opt. Exp.*, vol. 21, pp. 4740–4751, 2013.
[62] J. R. Koehler et al., "Post-recombination effects in confined gases photoionized at megahertz repetition rates," *Opt. Exp.*, vol. 29, pp. 4842–4857, 2021.
[63] T.-C. Truong et al., "Power scaling in N_2O-filled hollow-core fiber with helium buffer gas," in *Proc. Conf. Laser Electro-Opt.*, 2023, Paper STh1P.1.
[64] J. R. Koehler, D. Schade, P. S. J. Russell, and F. Tani, "Gas mixtures to suppress thermal buildup effects caused by high-repetition-rate photoionization of confined gases," in *Proc. Conf. Lasers Electro-Opt. Europe Eur. Quantum Electron.*, 2021, Paper cf_1_5.
[65] J. E. Miller, L. Stroud, and L. W. Brandt, "Compressibility of helium-nitrogen mixtures," *J. Chem. Eng. Data*, vol. 5, pp. 6–9, 1960.
[66] T. Popmintchev et al., "Bright coherent ultrahigh harmonics in the keV X-ray regime from mid-infrared femtosecond lasers," *Science*, vol. 336, pp. 1287–1291, 2012.
[67] T. Heuermann et al., "Ultrafast Tm-doped fiber laser system delivering 1.65-mJ, sub-100-fs pulses at a 100-kHz repetition rate," *Opt. Lett.*, vol. 47, pp. 3095–3098, 2022.
[68] L. Kiani et al., "High average power ultrafast laser technologies for driving future advanced accelerators," *J. Instrum.*, vol. 18, 2023, Art. no. T08006.
[69] Y. Wu et al., "Generation of few-cycle multi-millijoule 2.5 μm pulses from a single-stage Cr2+:ZnSe amplifier," *Sci. Rep.*, vol. 10, 2020, Art. no. 7775.
[70] V. E. Leshchenko et al., "High-power few-cycle Cr:ZnSe mid-infrared source for attosecond soft x-ray physics," *Optica*, vol. 7, pp. 981–988, 2020.
[71] Z. A. Marra, Y. Wu, F. Zhou, and Z. Chang, "Cryogenically cooled Fe:ZnSe-based chirped pulse amplifier at 4.07 μm," *Opt. Exp.*, vol. 31, pp. 13447–13454, 2023.

Tran-Chau Truong received the B.S. and M.Sc. degrees in physics from the Ho Chi Minh City University of Education, Ho Chi Minh City, Vietnam, in 2011 and 2013, respectively, and the Ph.D. degree in physics from the University of Central Florida, Orlando, FL, USA, in 2023, under the supervision of Prof. Micheal Chini. She is currently a Postdoctoral Researcher with the University of Central Florida. As of Fall 2024, she will move to The Ohio State University, where she will work as a Postdoctoral Researcher with the Department of Physics. Her research interests include the development of isolated attosecond sources and characterization tools for attosecond science, and studying electron dynamics in materials using novel attosecond time-resolved spectroscopy. She is also a Member of the American Physical Society and Optica.

Christopher Lantigua received the B.S. degree in electrical engineering from the University of Florida, Gainesville, FL, USA, in 2010, and the M.S. degree in optics in 2013 from the College of Optics and Photonics (CREOL), University of Central Florida, Orlando, FL, USA, where he is currently working toward the Ph.D. degree in physics. In 2022, he joined the LUMAS Group with the University of Central Florida, as a Research Assistant. He is also completing work for the Ph.D. dissertation with SLAC National Accelerator Laboratory under an Award from the Department of Energy. His research interests include, attosecond physics, ultrafast lasers science and its applications. Mr. Lantigua was the recipient of the Department of Energy, Office of Science Graduate Research (SCGSR) Program Award.

Yuxuan Zhang received the B.S. degree in physics from Xi'an Jiaotong University, Xi'an, China, in 2018, and the M.S. degree in materials design and innovation from the State University of New York at Buffalo, NY, USA, in 2020. He is currently working toward the Ph.D. degree with the Department of Physics, Binghamton University, Binghamton, NY, USA. His research interests include experimental laser-matter interactions and simulations. He is also the Member of American Physical Society.

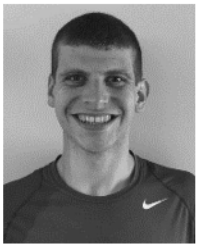

Jack W. Agnes received the B.A. degree in physics from SUNY Geneseo, Geneseo, NY, USA, in 2020. He is currently working toward the Ph.D. degree with Binghamton University, Binghamton, NY, USA. His research interests include femtosecond laser micromachining, visualization/measurement of nonlinear laser-matter interactions, and attosecond pulse generation. He is also the Member of American Physical Society.

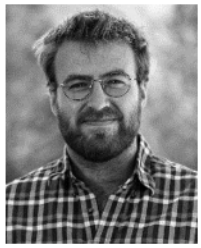

Ruaridh Forbes received the M.Sc. degree in chemical physics from the University of Edinburgh, Edinburgh, U.K., before starting graduate School with the University College London, London, U.K. The majority of his graduate work was carried out with the National Research Council of Canada under the supervision of Prof. Albert Stolow. He joined the Stanford PULSE Insitute as a Postdoctoral Scholar with the Group of Prof. Philip Bucksbaum before joining the Laser Science department of LCLS in 2020 to lead aspects of the LCLS II laser R&D Program. He is currently a Lead Scientist with the Linac Coherent Light Source (LCLS), SLAC National Accelerator Laboratory, Menlo Park, CA, USA. His research interests include experimental ultrafast spectroscopy, inner shell processes and strong-field physics in polyatomic molecules, and development of high average power and high repetition rate laser sources.

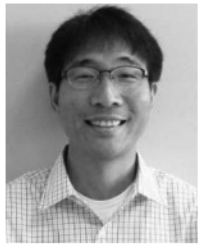

Bonggu Shim received the B.S. degree in physics from Seoul National University, Seoul, South Korea, in 1997, and the Ph.D. degree in physics from the University of Texas at Austin, TX, USA, in 2006. From 2006 to 2007, he was a Postdoctoral Researcher with the University of Texas at Austin and was a Postdoctoral Researcher with Cornell University, Ithaca, NY, USA, from 2007 to 2012. He is currently a Professor with the Department of Physics, Binghamton University, Binghamton, NY, USA. His research interests include experimental and theoretical high-intensity laser plasma interactions, femtosecond laser spectroscopy, atomic, molecular, optical physics, and high-power laser design and construction. Dr. Shim is also the Member of the American Physical Society and Optica.

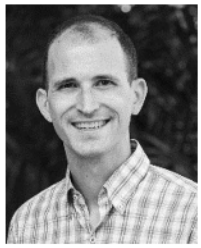

Michael Chini (Member, IEEE) received the B.S. degree in physics from McGill University, Montreal, QC, Canada, in 2007, and the Ph.D. degree in physics from the University of Central Florida, Orlando, FL, USA, in 2012, under the supervision of Prof. Zenghu Chang. He attended graduate school with Kansas State University, Manhattan, KS, USA, before transferring to University of Central Florida. From 2012 to 2014, he was a Postdoctoral Research Associate with the Institute for the Frontiers of Attosecond Science and Technology, University of Central Florida, where he then moved into the role of Senior Research Scientist in the Townes Laser Institute in 2014 and became Assistant Professor of Physics in 2015. He is currently an Associate Professor with the Department of Physics, with a secondary joint appointment in CREOL – The College of Optics and Photonics, University of Central Florida. As of Fall 2024, he will move his group to The Ohio State University, Columbus, OH, USA, where he will be Associate Professor with the Department of Physics. His research interests include the development of novel laser sources and technology for attosecond science, and the application of attosecond time-resolved spectroscopies to study laser-driven charge dynamics in gas-phase molecules and solid-state systems. Prof. Chini was the recipient of an Air Force Office of Scientific Research's Young Investigator Program Award and a Department of Energy Early Career Research Award. He is also the Fellow of Optica.